Plasma heating via parametric beating of Alfvén waves, with heliospheric applications

Steven H. Bekhor[a)]
Department of Nuclear Engineering, University of Michigan, Ann Arbor, Michigan 48109

R. Paul Drake
Department of Atmospheric, Oceanic and Space Science, University of Michigan, Ann Arbor, Michigan 48109

(Received 18 March 2003; accepted 29 July 2003)

This paper advances a novel mechanism to explain the dissipation of the Alfvén waves that carry much of the energy in heliospheric and astrophysical turbulence, with specific applications to solar wind heating. The essential point is that the nonlinear beating of relatively low-frequency Alfvén waves, which are abundant in the heliosphere, drives a compressible magnetosonic response whose damping can dissipate significant energy. This mechanism involves both kinetic and magnetohydrodynamic (MHD) processes. The damping of the magnetosonic waves is a kinetic process. The nonlinear beating of Alfvén waves, which produces the magnetosonic waves, is best described by MHD theory. This mechanism complements and may compete with the well-known alternative mechanism in which the cascade of turbulent energy to small-scale, high-frequency Alfvén waves dissipates by ion-cyclotron damping. The MHD analysis in this paper reveals that the fast magnetosonic mode dominates the dissipation when the plasma beta is near unity, and that the timescale of dissipation in the heliosphere can vary from hours to a year depending upon the direction of the driven wave and the plasma parameters where it is driven. The damping of the driven magnetosonic waves may also contribute to the observed high-energy particle distributions. [DOI: 10.1063/1.1619975]

I. INTRODUCTION

Alfvén waves have long been known to contribute significantly to the turbulence observed in interplanetary[1,2] and astrophysical[3] flows. However, it is not quite understood how the energy associated with these waves transmits itself in the form of dissipation due to large-scale interactions. This document examines a wave interaction mechanism whereby Alfvénic turbulence can dissipate,[4] with a particular focus on issues related to solar wind heating and acceleration.

Understanding the coronal expansion of matter, first addressed thoroughly by Parker, requires one or more mechanisms that can both account for the initial transition from subsonic to supersonic flow near 2 solar radii and explain the subsequent supersonic expansion that takes place at greater distances from the Sun.[5] Regardless of how the energy deposited in the corona and the solar wind is dissipated, it is believed to originate in the solar convection zone. As this energy is transported radially outward, it is subject to certain constraints. For one, in a flow that is assumed to be steady and in which viscosity is assumed to be negligible, the sum of the bulk flow energy, enthalpy, gravitational potential energy, thermal conduction flux and magnetohydrodynamic (MHD) wave flux is constant.[6] Second, the source of the flow energy associated with coronal or solar wind expansion, such as hot particles or MHD waves, must be sustained in order for an acceleration mechanism to take effect over large distances.

The medium surrounding the sun, the heliosphere, has long been known to undergo considerable heating as turbulence propagates outward to increasing heliocentric distances. Subsequent adiabatic cooling results in the outward expansion of the plasma and the acceleration of the solar wind. In particular, the plasma temperature increases from 5000 K at the surface of the sun to millions of degrees Kelvin in the corona and the solar wind.[7] Though this heating is known to occur, it is not understood precisely how the heat in the corona is dissipated on time scales of tens of minutes or how the subsequent heating occurs. For example, the critical points in the fast and slow solar winds are located at 2 and 5 solar radii, respectively. Thus, some of the energy that is produced in the transition layer between the photosphere and the corona is dissipated within these distances from the sun. Yet, Parker found that no bound oscillatory solutions exist inside the corona.[5]

Within the corona, this heating has been attributed to atomic emissions, thermal bremsstrahlung, magnetohydrodynamic instabilities and interactions between Alfvén waves and the sun's current sheet. Beyond the corona, various interactions among magnetohydrodynamic waves and ionized particles are believed to be responsible for the heating. Most current models of solar wind heating are based on the concept of turbulent cascades from ordinary hydrodynamic

[a)]Present address: Department of Physics, University of Alberta, Edmonton, Alberta T6G 2J1, Canada. Electronic mail: chalutz@umich.edu

theory. The cascade paradigm, whose description requires numerical simulation, describes the transmission of energy to increasing wave number. When a critical wave number is reached, that corresponding to the ion cyclotron frequency, the energy in the Alfvén waves is dissipated to the medium through resonant interactions.[1,2] This type of cascade followed by a resonant interaction has been explored thoroughly by members of the space physics community.

In the present paper, we examine analytically an alternative model, in which the nonlinear beating of relatively low-frequency Alfvén waves, which are abundant in the heliosphere, drives a compressible magnetosonic response whose damping dissipates significant energy. Magnetosonic waves are, after all, present in any MHD plasma and damp readily. Even though they are not observed at large amplitude, they may be the important pathway for energy dissipation. Though both this mechanism and the cascade mechanism should contribute to the heating of the solar wind, it is important to determine which mechanism is dominant and whether all of the heating observed in the heliosphere can be accounted for on theoretical grounds.

Some prior work is specifically relevant to the present discussion. Gravity damping of Alfvén waves in regions where the Alfvén speed is low was used to explain the heating of protons in the solar corona to several million degrees and the acceleration of the solar wind.[8,9] Statistical acceleration has been used in order to explain the presence of ubiquitous high energy tails in the solar wind.[10] Examination of compressible MHD interactions in one dimension leads to a kinetic nonlinear Schrödinger equation, which includes damped nonlinear Alfvénic turbulence that interacts with sound waves. Dissipative structures emerge due to the competition between the nonlinear steepening of the wave spectrum and collisionless damping.[11–13] The effects of broadband forcing due to a turbulent energy spectrum have been investigated using a simple MHD model. It was demonstrated that appropriate choices of plasma beta can recover the Kolmogorov and Kraichnan dissipation scales.[14,15] Most recently, it was demonstrated numerically that a turbulent cascade of fast magnetosonic waves occurs on shorter times scales than one involving Alfvén or slow magnetosonic waves, which are weakly coupled.[16,17] Previous work has also been done in the development of a wave coupling formalism for MHD waves and the study of instabilities involving large-amplitude Alfvén waves.[18]

II. THE PHYSICAL BASIS FOR THE NONLINEAR MECHANISM

The nonlinear problem of interest is an example of a parametric process, whose first-order signal waves, the driven magnetosonic response, are coupled to a pair of interacting Alfvén pump waves. As parametric beating takes place, the damping of magnetosonic waves leads to the depletion of the Alfvén waves, altering their amplitudes and characteristics. Furthermore, the first-order signal is, in reality, coupled to processes of even higher order. Our approach assumes that the higher-order processes are negligible compared to the Alfvén wave interaction and magnetosonic wave damping and that the shape, phase, and amplitude of the signal or driven wave does not change drastically over the correlation time of the longest Alfvén wavelength considered in this calculation.[19]

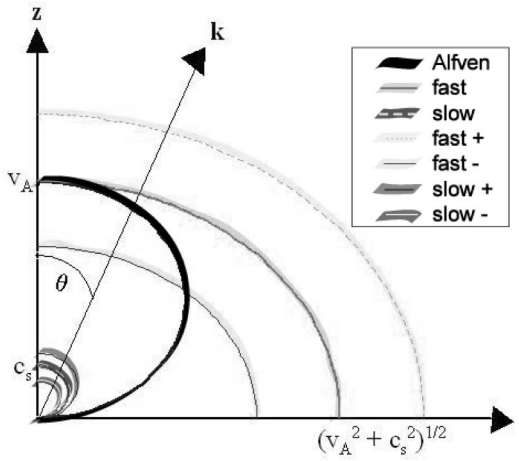

FIG. 1. Polar representation of Alfvén and magnetosonic (fast, furthest from the axis, and slow, closest to the axis) dispersion relations. ($v_A > c_s$) The dashed lines reflect resonance broadening due to the presence of damping. z is the direction of the mean magnetic field.

Prior to entering into any detailed discussion of the mechanism at hand, it is worthwhile to understand how parametric beating, the nonlinear beating of specified amplitudes which drive a third amplitude, can lead to robust power loss in the presence of strong damping. Driven waves involved in a three-wave parametric interaction satisfy the following frequency, ω, and wave vector, $\mathbf{k}$, matching conditions. The quantities bearing indices are associated with the pump waves, whereas those without indices are associated with the driven waves:

$$\omega = \pm\omega_i \pm \omega_j = (\pm k_{zi} \pm k_{zj}) v_A = k_z v_A \tag{1}$$

and

$$\mathbf{k} = \pm\mathbf{k}_i \pm \mathbf{k}_j . \tag{2}$$

This is known as phase matching. At resonance, the driven waves are prescribed by the matching conditions in accordance with the wave numbers and frequencies of the driving normal modes. When the pump modes are expressed in terms of wave packets, a range of pump wave vectors and frequencies may excite a broad spectrum of driven waves. However, the strongest response always occurs when the driven wave vectors and frequencies nearly satisfy the resonant dispersion relation for a naturally occurring mode in the plasma. In other words, the strongest driven mode has a phase velocity corresponding to the group velocity of the wave packet. When damping is present, the domain over which the driven waves are nearly resonant is broadened.

Figure 1 shows, in the form of phase speed versus propagation angle, the dispersion relations of the Alfvén wave and the fast and slow magnetosonic waves. It can be used to illustrate the interactions that are possible between two Alfvén pump waves and a magnetosonic signal wave. For the present case when both driving waves are Alfvénic, it

turns out that Eq. (1) is redundant with the parallel component of Eq. (2). This has the implication that waves that are driven at resonance must satisfy the dispersion relation for torsional Alfvén waves. Thus, the Alfvén waves interact most strongly with the magnetosonic waves when the thick solid curve in Fig. 1 approaches one of the magnetosonic curves.

Damping of the magnetosonic waves, first addressed by Barnes,[20] leads to an effective broadening of the domain, shown by dashed lines, over which interacting waves are nearly resonant. For illustrative purposes, the damping coefficient, Γ/ω, is chosen to be 0.3 in Fig. 1 for both the slow and fast modes. The effect of the presence of damping in any model of a plasma on the phase speeds of the normal modes will be addressed in Sec. IV. It is precisely this off-resonant beating that allows a large number of beat (ij) products to contribute to the overall magnetosonic response. As can be seen in the figure, the fast magnetosonic mode beats efficiently with Alfvén waves when its phase speed approaches the Alfvén speed. This occurs when the fast mode propagates in a direction that is nearly parallel to the mean magnetic field. Interactions involving this wave experience some broadening due to a small associated damping coefficient. On the other hand, the slow mode is far from the Alfvén resonance except when it propagates in a direction that is perpendicular to the mean magnetic field or when the plasma beta approaches unity. Unfortunately, there is no wave energy associated with the zero-frequency amplitude. The strong damping associated with the slow mode permits some nearly perpendicular waves to beat with the Alfvén pump waves. However, the response is relatively weak. Therefore, most of the energy associated with the mechanism described in this work is derived from the fast magnetosonic response, except when the plasma beta approaches unity. The effective rate at which this energy is dissipated to the solar wind particles is quantified in the following sections.

III. THE MHD EQUATIONS

The ideal magnetohydrodynamic equations are the point of departure for the detailed calculations:

$$\partial_t \rho + \nabla\cdot(\rho\mathbf{u}) = 0, \tag{3}$$

$$\rho\partial_t\mathbf{u} + \rho(\mathbf{u}\cdot\nabla)\mathbf{u} = -c_s^2\nabla\rho + \frac{1}{\mu_0}(\nabla\times\mathbf{B})\times\mathbf{B} \tag{4}$$

and

$$\partial_t\mathbf{B} = \nabla\times(\mathbf{u}\times\mathbf{B}), \tag{5}$$

where ρ, $\mathbf{u}$, and $\mathbf{B}$ denote the mass density, velocity, and magnetic field associated with the fluid, ∂_t is a partial derivative in time, c_s is the speed of sound, and μ_0 is the permeability of free space. A cursory inspection of Eq. (4) already yields some preliminary information about hydrodynamic waves. The left-hand side of this equation represents first- and second-order fluctuations associated with the kinetic energy of the particles. These are coupled to compressional and magnetic fluctuations on the right-hand side of the equation. Moreover, the first term on the right-hand side, associated with compressible fluctuations, drives fluctuations in the fluid velocity, which are purely longitudinal to first order. On the other hand, the second term, associated with magnetic fluctuations, drives first-order fluid-velocity fluctuations that are orthogonal to both the magnetic field and the current density.

The calculation has been carried out in Fourier space in order to avoid the usual complications associated with solving a system of differential equations of high order. Beginning with the ideal magnetohydrodynamic equations describing a plasma, the second- and higher-order couplings of two pump waves, either Alfvén or magnetosonic, to first-order driven waves are considered. Upon identifying the relevant driving and driven terms in the resulting equation, the solution for the first-order driven velocity is obtained in terms of the higher-order quantities. Subsequently, energy densities and energy extraction rates can be calculated.

The couplings can be observed upon making the following perturbative expansion about the dynamical quantities in the ideal MHD equations. Terms with the subscript 0 are defined as the average quantities in the expansion, whereas all others are first-order perturbative quantities representing the sum of all Alfvénic (A) and magnetosonic (M) fluctuations present in the physical system under consideration:

$$\rho = \rho_0 + \rho_1, \tag{6}$$

$$\mathbf{u} = \mathbf{u}_A + \mathbf{u}_M, \tag{7}$$

and

$$\mathbf{B} = \mathbf{B}_0\hat{\mathbf{e}}_z + \mathbf{B}_A + \mathbf{B}_M, \tag{8}$$

where $\hat{\mathbf{e}}_z$ is a unit vector along the static magnetic field, which is chosen to lie along the z axis. The zero-order velocity, which would produce a Doppler shift in the resulting equations, is ignored.

Alfvénic fluctuations in a hot magnetoplasma are defined by the following incompressibility condition, $\nabla\cdot\mathbf{u}_A = 0$. Magnetosonic fluctuations are, on the other hand, compressible. Both, however, share the property that particles move with the ripples in magnetic field lines. This property is a consequence of Eq. (5), which is often referred to as the frozen-in law.

In order to solve the system of Eqs. (3)–(5), an additional time derivative is applied to Eq. (4). This allows the immediate substitution of Eqs. (3) and (5) into Eq. (4). The overall structure of the equation after making the above substitutions and eliminating the dynamical variables, ρ_1, $\mathbf{B}_A$, and $\mathbf{B}_M$, appearing in first-order terms among the three equations, is as follows:

$$\mu_0\rho_0(D_A^2\mathbf{u}_A+\mathbf{D}_M^2\cdot\mathbf{u}_M)=\text{second- and third-order coupling terms}$$

$$=\nabla\left[\mathbf{B}_0\cdot\left(\sum_{g=A,M}\mathbf{B}_g\nabla\cdot\mathbf{u}_M+\sum_{f=A,M}\sum_{g=A,M}[(\mathbf{u}_f\cdot\nabla)\mathbf{B}_g-(\mathbf{B}_f\cdot\nabla)\mathbf{u}_g]\right)\right]$$

$$-B_0\partial_z\left(\sum_{g=A,M}\mathbf{B}_g\nabla\cdot\mathbf{u}_M+\sum_{f=A,M}\sum_{g=A,M}[(\mathbf{u}_f\cdot\nabla)\mathbf{B}_g-(\mathbf{B}_f\cdot\nabla)\mathbf{u}_g]\right)-\frac{1}{2}\partial_t\sum_{f=A,M}\sum_{g=A,M}\nabla(\mathbf{B}_f\cdot\mathbf{B}_g)$$

$$+\partial_t\sum_{f=A,M}\sum_{g=A,M}(\mathbf{B}_f\cdot\nabla)\mathbf{B}_g+\mu_0\sum_{g=A,M}[c_s^2\nabla(\nabla\cdot(\rho_1\mathbf{u}_g))-\partial_t(\rho_1\partial_t\mathbf{u}_g)]$$

$$-\mu_0\rho_0\partial_t\sum_{f=A,M}\sum_{g=A,M}(\mathbf{u}_f\cdot\nabla)\mathbf{u}_g-\mu_0\partial_t\rho_1\sum_{f=A,M}\sum_{g=A,M}(\mathbf{u}_f\cdot\nabla)\mathbf{u}_g, \tag{9}$$

where D_A^2 and $\mathbf{D}_M^2$ denote the dispersion operators for Alfvén and magnetosonic waves, respectively. The summations are over the Alfvén and magnetosonic indices. It is worthwhile to note that the continuity equation only enters into the compressive magnetosonic wave dispersion relation to first order and not into the first-order torsional Alfvén wave dispersion relation.

The development of Eq. (9) is similar to an earlier analysis by Goldstein, except for the fact that first-order quantities are not assumed to vary only along $\mathbf{B}_0$ and the Alfvén pump waves are chosen to be linearly rather than circularly polarized.[21] In addition, Eq. (9) includes higher-order interactions with magnetosonic waves. The limitation to a ''slab geometry'' is relaxed in subsequent papers in which monochromatic large-amplitude circularly polarized Alfvén waves are coupled to electromagnetic daughter waves via the numerical solution of a system of linearized equations.[22,23] Unlike most past work, which has examined the behavior of a single, initial, large-amplitude wave, we consider here the effects that may be produced through the interaction of many waves of a more modest amplitude. The dispersion operators are defined as follows:

$$D_A^2(\mathbf{x},t)\mathbf{u}(\mathbf{x},t)=\partial_t^2\mathbf{u}-\mathbf{v}_A^2\partial_z^2\mathbf{u} \tag{10}$$

and

$$\mathbf{D}_M^2(\mathbf{x},t)\cdot\mathbf{u}(\mathbf{x},t)=\partial_t^2\mathbf{u}-\mathbf{v}_A^2\partial_z^2\mathbf{u}+v_A^2\nabla(\partial_z u_z)+v_A^2\hat{\mathbf{e}}_z\partial_z(\nabla\cdot\mathbf{u})-(v_A^2+c_s^2)\nabla(\nabla\cdot\mathbf{u}), \tag{11}$$

where

$$v_A^2=\frac{B_0^2}{\mu_0\rho_0}, \tag{12}$$

$$c_s^2=\frac{5}{3}\frac{P_0}{\rho_0}, \tag{13}$$

v_A is the zero-order Alfvén speed and P_0 is the zero-order pressure.

The usual dispersion relations for the fast and slow modes, in addition to their coupling to Alfvén waves, is obtained as follows. The entire expression consisting of first-order driven quantities and higher-order driving terms, Eq. (9), is Fourier transformed. The dispersion operators in Fourier space are as follows, where **1** is the unit dyadic:

$$D_A^2(\mathbf{k},\omega)=-\omega^2+k_z^2v_A^2 \tag{14}$$

and

$$\mathbf{D}_M^2(\mathbf{k},\omega)=-[(\omega^2-k_z^2v_A^2)\mathbf{1}+\mathbf{v}_A^2k_z(\mathbf{k}\hat{\mathbf{z}}+\hat{\mathbf{z}}\mathbf{k})-(v_A^2+c_s^2)\mathbf{k}\mathbf{k}]. \tag{15}$$

It is important to note that in this section, $\mathbf{D}_M^2$ operates as a tensor, rather than a scalar. Upon choosing the following spherical representation for the wave number,

$$\frac{\mathbf{k}}{k}=\sin\theta\cos\phi\hat{\mathbf{x}}+\sin\theta\sin\phi\hat{\mathbf{y}}+\cos\theta\hat{\mathbf{z}}, \tag{16}$$

we obtain

$$\mathbf{D}_M^2(\mathbf{k},\omega)=-\begin{pmatrix}\omega^2-k^2v_A^2\cos^2\theta-k^2(c_s^2+v_A^2)\sin^2\theta\cos^2\phi & -k^2(c_s^2+v_A^2)\sin^2\theta\sin\phi\cos\phi & -k^2c_s^2\cos\theta\sin\theta\cos\phi\\ -k^2(c_s^2+v_A^2)\sin^2\theta\sin\phi\cos\phi & \omega^2-k^2v_A^2\cos^2\theta-k^2(c_s^2+v_A^2)\sin^2\theta\sin^2\phi & -k^2c_s^2\cos\theta\sin\theta\sin\phi\\ -k^2c_s^2\cos\theta\sin\theta\cos\phi & -k^2c_s^2\cos\theta\sin\theta\sin\phi & \omega^2-k^2c_s^2\cos^2\theta\end{pmatrix}. \tag{17}$$

At this point, we define $v_{\mathrm{ph}}=\omega|_{\lambda=0}/k$, the usual phase velocities of the MHD modes, where λ denotes an eigenvalue of $\mathbf{D}_M^2$, and $\hat{\mathbf{x}}$, $\hat{\mathbf{y}}$ and $\hat{\mathbf{z}}$ are unit vectors in the Cartesian coordinate system. The matrix in Eq. (17) is symmetric and is, therefore, orthogonally diagonalizable for all values of θ and ϕ.[24] The resulting eigenvalues are

$$\lambda_0=-\omega^2+k^2v_A^2\cos^2\theta, \tag{18}$$

$$\lambda_N=-\omega^2+\frac{1}{2}k^2[c_s^2+v_A^2 + (-1)^N\sqrt{(c_s^2+v_A^2)^2-4c_s^2v_A^2\cos^2\theta}]. \tag{19}$$

Dispersion relations for all modes can be obtained by setting $\lambda=0$, with Eq. (18) giving the usual Alfvén waves and Eq. (19) the usual magnetosonic waves.[25] Upon invoking this equality, we can determine the phase velocities for the torsional Alfvén and the fast and slow magnetosonic waves, respectively. The eigenvector, $\mathbf{u}_0$, associated with λ_0 appears in the following equation:

$$\mathbf{u}_0\propto-\sin\phi\hat{\mathbf{x}}+\cos\phi\hat{\mathbf{y}}, \tag{20}$$

whereas those associated with λ_N, $\mathbf{u}_N$, can be computed using either of the following equations:

$$\mathbf{u}_N\propto\left[\frac{v_{\mathrm{ph}}^2}{c_s^2}-\cos^2\theta\right](\cos\phi\hat{\mathbf{x}}+\sin\phi\hat{\mathbf{y}})+\sin\theta\cos\theta\hat{\mathbf{z}} \tag{21}$$

or

$$\mathbf{u}_N\propto\sin\theta\cos\theta(\cos\phi\hat{\mathbf{x}}+\sin\phi\hat{\mathbf{y}})+\left[\frac{v_{\mathrm{ph}}^2-v_A^2}{c_s^2}-\sin^2\theta\right]\hat{\mathbf{z}}. \tag{22}$$

Equations (21) and (22) are valid for both the fast and slow magnetosonic modes and can be shown to be mathematically equivalent. However, Eq. (21) is indeterminate in the limits of parallel and perpendicular propagation for the slow mode and Eq. (22) is indeterminate in the same limits for the fast mode. Regardless, the application of l'Hopital's rule recovers the correct ratio between the parallel and perpendicular components of the fluctuating velocities in all four cases.

The determination of the driven fluctuating magnetosonic and Alfvén velocities can be completed by eliminating ρ_1, $\mathbf{B}_A$, and $\mathbf{B}_M$ using the relations

$$\frac{\rho_1}{\rho_0}=\hat{\mathbf{k}}\cdot\frac{\mathbf{u}_M}{v_{\mathrm{ph}M}}, \tag{23}$$

$$\frac{\mathbf{B}_A}{B_0}=-\frac{\mathbf{u}_A}{v_A}, \tag{24}$$

and

$$\frac{\mathbf{B}_M}{B_0}=(\hat{\mathbf{z}}\hat{\mathbf{k}}-\cos\theta\mathbf{1})\cdot\frac{\mathbf{u}_M}{v_{\mathrm{ph}M}}, \tag{25}$$

where $v_{\mathrm{ph}M}$ is the phase velocity of magnetosonic waves, and, ultimately, dividing by the appropriate dispersion relation.

IV. THE DESCRIPTION OF THE DAMPED, DRIVEN MODES

We address here the specific example of the beating of Alfvén waves, which results in the production of fast and slow magnetosonic waves. The reasonable underlying assumption is that the decay time of these driven waves is short compared to the correlation time of the Alfvén waves. In particular, the energy density associated with each mode is computed using known expressions. Finally, the role of this mechanism in the process of solar wind heating is explored by evaluating the effective damping rate associated with the overall mechanism. For the purpose of this discussion, the Alfvén wave turbulence is assumed to have a simple plane wave structure. This approach allows one to obtain a value for the effective damping rate without resorting to numerical integration. However, the turbulence encountered in the heliosphere, in fact, has a more complicated structure, which might often be approximated as the sum of Gaussian wave packets, on length scales that are greater than or equal to the order of the correlation length of the turbulence.

In order to allow for the broad spectrum of the Alfvénic turbulence, we represent the pump waves as a sum of many components, each of which is a plane wave. The complex representation of a summation of H real plane waves with constant complex root-mean-squared (rms) amplitudes, w_h, frequencies, ω_h, and wave numbers, $\mathbf{k}_h$, is

$$w(\mathbf{x},t)=\frac{1}{2\sqrt{H}}\sum_{h=1}^{H}\sum_{m=\pm1}[\mathrm{Re}(w_h)+im\,\mathrm{Im}(w_h)] \times\exp(-im\omega_h^{(m)}t+im\mathbf{k}_h\cdot\mathbf{x})\exp(im\phi_h). \tag{26}$$

The factor in the denominator is due to the fact that the rms amplitude for H independent amplitudes scales as the rms total amplitude divided by $\sqrt{H}$. In the event that $w(\mathbf{x},t)$ happens to be a vector, w_h is also associated with a direction. The sum over m accounts for complex conjugate pairs. The bracketed subscript above the omega is a convention used to denote conjugate pairs. $(+)$ denotes a value that is not conjugated. $(-)$ denotes the conjugate of the former. The constant exponential term, $\exp(im\phi_h)$, is an arbitrary phase.

As Landau damping is absent from the fluid description of plasmas, it is necessary to incorporate such damping phenomenologically. One standard way to reflect the rapid damping of magnetosonic waves compared to that associated with Alfvén waves is to add an artificial damping term to the dispersion relation. The damping rate for magnetosonic waves varies as a function of the phase speed. However, one may be inclined to approximate the damping coefficient, Γ/ω, using a constant or polynomial in analogy to collisional damping. In either case, Γ/ω must be evaluated or approximated outside the context of MHD theory. This is a standard approach in problems involving fluid theories and is undertaken below. The inclusion of this damping in Eq. (11) yields

$$\mathbf{D}_M^2\cdot\mathbf{u}(\mathbf{x},t)=\partial_t^2\mathbf{u}+2\Gamma\partial_t\mathbf{u}-v_A^2\partial_z^2\mathbf{u}+v_A^2\nabla(\partial_z u_z) + v_A^2\hat{\mathbf{e}}_z\partial_z(\nabla\cdot\mathbf{u})-(v_A^2+c_s^2)\nabla(\nabla\cdot\mathbf{u}). \tag{27}$$

The undamped Alfvénic dispersion operator, D_A^2, remains the same. The analogous expression for $\mathbf{D}_M^2$ in Fourier space is

$$\mathbf{D}_M^2(\mathbf{k},\omega) = -[(\omega[\omega + 2i\Gamma] - k_z^2 v_A^2)\mathbf{1} + v_A^2 k_z(\mathbf{k}\hat{\mathbf{z}} + \hat{\mathbf{z}}\mathbf{k}) - (v_A^2 + c_s^2)\mathbf{k}\mathbf{k}]. \tag{28}$$

Since $\mathbf{D}_M^2$ is orthogonally diagonalizable, we can use the eigenvectors obtained in Eqs. (20)–(22) in order to construct an orthonormal basis[24] for R^3. Therefore, any vector $\mathbf{u}$ in R^3 can be represented as a linear combination of this set of unit vectors, denoted by the caret, according to the following Galerkin method:

$$\mathbf{u} = \sum_{N=1}^{2} c_N \hat{\mathbf{u}}_N + c_0 \hat{\mathbf{u}}_0 . \tag{29}$$

The amplitudes, c_N and c_0, represent the components of $\mathbf{u}$ in each orthogonal direction and add in quadrature. Upon adopting this representation and acknowledging that all the dynamical variables can be expressed in terms of $\mathbf{u}_A$, whose dispersion relation is prescribed by $D_A^2 = 0$, and $\mathbf{u}_M$, Eq. (9) can be written in the following manner, where $\mathbf{O}_{2A}$ and $\mathbf{O}_{2M}$ are nonlinear tensor operators:

$$\mathbf{D}_M^2|\mathbf{u}\rangle = \mathbf{O}_{2A}|\mathbf{u}_A\rangle + \mathbf{O}_{2M}|\mathbf{u}_M\rangle. \tag{30}$$

The amplitudes c_0 and c_N can immediately be calculated from Eq. (30) by premultiplying it by the complex conjugates of the unit vectors $\hat{\mathbf{u}}_0$ and $\hat{\mathbf{u}}_N$ and dividing by the associated eigenvalue:

$$c_i = \frac{\langle \hat{\mathbf{u}}_i|\mathbf{O}_{2A}|\mathbf{u}_A\rangle}{\lambda_i} + \frac{\langle \hat{\mathbf{u}}_i|\mathbf{O}_{2M}|\mathbf{u}_M\rangle}{\lambda_i}. \tag{31}$$

Returning to the eigenvalues of Eq. (28) associated with the magnetosonic waves, these can be rewritten in the following convenient and compact form upon factoring and rearranging:

$$\lambda_N = -(1+2ib)\prod_{Z=1,2}(\omega + kap(Z,N)), \tag{32}$$

where

$$p(Z,N) = \frac{(-1)^Z}{\sqrt{2}} \times \sqrt{c_s^2 + v_A^2 + (-1)^N \sqrt{(c_s^2 + v_A^2)^2 - 4\frac{k_z^2}{k^2} c_s^2 v_A^2}}, \tag{33}$$

$$a = \frac{\sqrt{1+\sqrt{1+4b^2}} - \sqrt{1-\sqrt{1+4b^2}}}{\sqrt{2}\sqrt{1+4b^2}}, \tag{34}$$

and

$$b = \frac{\Gamma}{\omega}. \tag{35}$$

The expression, p, as written, is the phase velocity at which undriven and undamped magnetosonic waves propagate. It varies as a function of $\mathbf{k}$. Equations (32) and (33) reveal the usual fast ($N=2$) and slow ($N=1$) modes, traveling forward ($Z=1$) and backward ($Z=2$). In addition, the resistive damping introduced in Eq. (27) appears not only to have added imaginary terms to the roots of the dispersion relation. The respective phase velocities for the fast and slow magnetosonic waves have also been shifted downward. For example, when $b=0.3$, the phase velocities are reduced to 89% of their undamped values. As can be seen in the work of Barnes,[20] the inclusion of Landau damping using kinetic theory does indeed produce a shift in the real phase velocities of the magnetosonic waves. However, in light of the earlier discussion of parametric beating, resistive damping does not only broaden the resonances associated with these interactions. It also shifts the frequencies at which phase matching can occur downward, producing two effects. It alters the combinations of Alfvén waves that most strongly drive a magnetosonic response as well as the strength of the response unless Alfvén wave damping is introduced in a consistent manner.

In addition, the introduction of a constant damping rate does not include the variation in the strength of the Landau damping associated with the different magnetosonic modes. In order to reflect the dependence of the energy density on frequency and wave number, the variation in the strength of the damping must be included in the calculation. On the other hand, the dispersion relations appearing in Eq. (32) are not entirely useless. In regimes where collisional damping is important, they may be used to calculate the heating in a manner analogous to the one that follows.

The introduction of resistive damping does, however, inform us about how damping manifests itself in the dispersion relation. Because Landau damping is different for the fast and slow magnetosonic modes and the sign of the damping ratio differs for modes propagating in opposite directions, Eq. (32) cannot be used to reflect damping that depends on the angle of propagation simply by permitting Γ to vary. Instead, the appropriate imaginary terms may be added directly to the roots of the dispersion relation. A suitable introduction of such terms into Eq. (32) in congruence with the distinctiveness of the fast and slow modes follows for the perpendicular dispersion operator, where Γ has been set to 0:

$$\lambda_N = -\prod_{Z=1,2}(\omega + k[1 + id_{ZN}(\eta)]p(Z,N)), \tag{36}$$

where

$$d_{ZN}(\eta) = d_{ZN0} + d_{ZN1}\eta(\theta) + d_{ZN2}\eta^2(\theta) + d_{ZN3}\eta^3(\theta) \tag{37}$$

and

$$\eta(\theta) = \cos(\theta). \tag{38}$$

In this particular treatment, we have chosen to approximate the damping factor, $d_{ZN}(\eta)$, using a third degree polynomial. In the above representation, $d_{ZN}(\eta)p(Z,N) > 0$ is implicit in order to reflect the damping rather than the growth of the driven waves. As long as the nearly resonant contributions to the driven fluctuations are more important than those that are considerably off resonance, the damping factor

TABLE I. Damping ratios for magnetosonic waves. The range of damping ratios for all angles of propagation is provided along with the rates corresponding to resonant peaks.

Plasma beta	d_{21}	d_{22}	d_{22} (resonant)
0.2	N/A	0.0001–0.03	0.0001
1	0.5–0.6	0.001–0.05	0.009
5	0.1–0.7	0.01–0.5	N/A

may be approximated by its values at resonance. In most cases, this is the damping rate associated with the fast magnetosonic wave, which is resonant with the Alfvén pump for parallel angles of propagation. Since there are no three-Alfvén-wave interactions, the most robust response occurs very slightly away from this resonance. On the other hand, when the plasma beta approaches unity, the slow mode also participates strongly in the interaction. Once again, the most robust response occurs when there is a partial resonance. In other words, the strongest response occurs when the real parts of the phase velocities are matched.

Barnes first presented an accurate calculation of the Landau damping of resonant magnetosonic waves for all directions of propagation and polarizations.[20] We fit $d_{ZN}(\eta)$ to the plots appearing in Fig. 3 of his paper for an isotropic plasma with $\beta=\mu_0 P_0/B_0^2=1$. The results are shown in Table I. The real parts of the magnetosonic phase velocities could be corrected in a similar manner by fitting them to the plots appearing in Fig. 4 of the Barnes paper using another polynomial. It can be seen immediately that the Vlasov theory predicts phase velocities that are smaller than those obtained using MHD and Chew–Goldberger–Low (CGL) theory. Although this correction would yield a more accurate expression for the energy density, it is unnecessary as long as the Alfvén and magnetosonic phase velocities are introduced into the problem in the same manner, thereby reflecting phase matching in a physically consistent way. We, therefore, use the real phase velocities obtained from the MHD theory to describe the waves.

V. THE EVALUATION OF THE ENERGY DENSITY ASSOCIATED WITH ALFVÉN–ALFVÉN MODE BEATING

Since this paper addresses the production of magnetosonic waves due to the second-order interaction of Alfvén waves, attention is only directed to the relevant terms in Eq. (9). Moreover, the other terms are beat products involving magnetosonic fluctuations, whose amplitude is small compared to the Alfvénic fluctuations in space plasmas according to nearly incompressible MHD.[26] In most cases, this condition is, at the very least, marginally satisfied. However, assuming that neither wave nor structure is monochromatic, but is composed of many fluctuations with randomly distributed wave numbers and phases, the small amplitude assumption for each single fluctuation should be satisfied.[27] Therefore, the contributions of these terms are dwarfed by the Alfvén–Alfvén interaction. The precise three-wave interaction that will be examined here is

$$\mathbf{D}_M^{2\prime}\cdot\mathbf{u}_M'=-\frac{\gamma^4}{8H}\sum_{h=1}^{H}\sum_{j=1}^{H}\sum_{m=\pm1}\sum_{n=\pm1}\omega\mathbf{k}\exp(i(m\phi_h+n\phi_j))\,\delta^3(\mathbf{k}-m\mathbf{k}_h-n\mathbf{k}_j)\,\delta(\omega-m\omega_h-n\omega_j)\times([\mathrm{Re}(\mathbf{u}_{Ah})+im\,\mathrm{Im}(\mathbf{u}_{Ah})]\cdot[\mathrm{Re}(\mathbf{u}_{Aj})+in\,\mathrm{Im}(\mathbf{u}_{Aj})]). \tag{39}$$

The right-hand side of Eq. (39) is the net Alfvén–Alfvén interaction term from Eq. (9). The left-hand side of Eq. (39) contains the scalar product of the dispersion operator, $\mathbf{D}_M^{2\prime}$, obtained using the polynomial fit to the damping rate from kinetic theory and the unknown magnetosonic response, $\mathbf{u}_M'$. $\mathbf{D}_M^{2\prime}$ is defined in terms of the eigenvalues in Eqs. (39) and (36) and the eigenvectors in Eqs. (20)–(22) as follows:

$$\mathbf{D}_M^{2\prime}=\mathbf{P}\cdot\mathbf{D}\cdot\mathbf{P}^T, \tag{40}$$

where

$$\mathbf{P}=\begin{bmatrix}\mathbf{u}_0 & \mathbf{u}_1 & \mathbf{u}_2\end{bmatrix} \tag{41}$$

and

$$\mathbf{D}=\begin{bmatrix}\lambda_0 & 0 & 0\\ 0 & \lambda_1 & 0\\ 0 & 0 & \lambda_2\end{bmatrix}. \tag{42}$$

$\mathbf{P}$ is a matrix containing the eigenvectors obtained by diagonalizing $\mathbf{D}_M^2$ and $\mathbf{D}$ is a diagonal matrix containing the eigenvalues. It should be noted that Eq. (39) is the governing equation that will be used in the remainder of this discussion.

Equation (39) clearly demonstrates that the second order Alfvén–Alfvén coupling drives a wave whose fluctuating velocity is in the direction defined by $\mathbf{k}=\mathbf{k}_h\pm\mathbf{k}_j$. All directions of propagation with respect to $\mathbf{u}_N$ are possible for both fast and slow magnetosonic waves. Here, N can designate either wave. However, $\mathbf{k}$ and $\mathbf{u}_0$ are always perpendicular for Alfvén waves. Thus, we deduce that the driven wave in Eq. (39) is purely magnetosonic. No Alfvén signal waves are driven as a result of Alfvén–Alfvén pump wave interactions based upon the assumptions made in this paper.

The resulting fluctuating velocity amplitudes of the driven magnetosonic waves in Fourier space can be calculated by dividing the orthogonal components on the right-hand side of Eq. (39) by the set of eigenvalues represented in Eq. (36). The velocity in configuration space can be used to calculate the total energy density resulting from the interaction as follows upon summing over the fast and slow modes, N, appearing below and the plane waves, h and j, and complex conjugates, m and n, in Eq. (39):

$$\varepsilon_M=\lim_{\tau\to\infty}\frac{(2\pi)^3}{2\gamma^6}\frac{M}{V^2\tau}\int d^3k\int_{-\infty/2}^{\infty/2}d\omega\times\sum_{N=1}^{2}C_{MN}(\theta,\phi)\,|c_N(\mathbf{k},\omega)|^2. \tag{43}$$

The amplitudes, c_N, are defined in Eq. (31). $C_{MN}(\theta,\phi)$ is the ratio of the total magnetosonic energy density to the kinetic magnetosonic energy density and can be derived using Eqs. (3)–(5) in conjunction with the magnetosonic dispersion relations:

$$C_{MN}(\theta,\phi)=1+\frac{2(v_A^2\sin^2\alpha_N[\cos^2\theta+\sin^2\theta\cos^2(\phi-\beta_N)]+c_s^2[\cos\theta\cos\alpha_N+\sin\theta\sin\alpha_N\cos(\phi-\beta_N)]^2)}{c_s^2+v_A^2+(-1)^N[(c_s^2+v_A^2)^2-4c_s^2v_A^2\cos^2\theta]^{1/2}}, \tag{44}$$

where

$$\alpha_N=\arccos\frac{u_{Nz}}{|\mathbf{u}_N|} \tag{45}$$

and

$$\beta_N=\arctan\frac{u_{Ny}}{u_{Nx}}=\phi \tag{46}$$

are the polar and azimuthal angles describing the direction of $\mathbf{u}_N$ with respect to $\mathbf{B}_0$. Equation (41) is used to calculate the effective coupling of energy from the Alfvén waves to the magnetosonic waves. The ratio of the driven energy density to that of the pump waves defines a coupling efficiency. The desired dissipation rate, ξ_M, is obtained by multiplying this efficiency by the damping rate for magnetosonic waves at each coordinate in configuration space:

$$\xi_M=\lim_{\tau\to\infty}\frac{(2\pi)^3}{\gamma^6}\frac{\rho_0}{V\tau}\int d^3k\int_{-\infty/2}^{\infty/2}d\omega\sum_{N=1}^{2}\Gamma_N(\mathbf{k},\omega)C_{MN}(\theta,\phi)|c_N(\mathbf{k},\omega)|^2, \tag{47}$$

where

$$\Gamma_N(\mathbf{k},\omega)=\mathrm{Im}(\omega)=d_{2N}(\eta)|\mathrm{Re}(\omega)|. \tag{48}$$

Upon invoking Eq. (47), we obtain the following, where $\omega_{hjmn}=m\omega_h+n\omega_j$ and $\mathbf{k}_{hjmn}=m\mathbf{k}_h+n\mathbf{k}_j$:

$$\begin{aligned}\xi_M=&\frac{\rho_0}{64H^2}\sum_{h=1}^{H}\sum_{j=1}^{H}\sum_{k=1}^{H}\sum_{l=1}^{H}\sum_{m=\pm1}\sum_{n=\pm1}\sum_{q=\pm1}\sum_{r=\pm1}\sum_{N=1}^{2}C_{MN}(\mathbf{k}_{hjmn})\times d_{2N}(\eta[\mathbf{k}_{hjmn}])|\omega_{hjmn}|^3\\&\times\exp(i(m\phi_h+n\phi_j-q\phi_k-r\phi_l))\frac{|\hat{\mathbf{u}}_N\cdot\mathbf{k}_{hjmn}|^2\delta_{\mathbf{k}_{hjmn},\mathbf{k}_{klqr}}\delta_{\omega_{hjmn},\omega_{klqr}}}{\Pi_{Z=1}^2|\omega_{hjmn}+|\mathbf{k}_{hjmn}|[1+id_{ZN}(\eta[\mathbf{k}_{hjmn}])]p(Z,N)|^2}\\&\times([\mathrm{Re}(\mathbf{u}_{Ah})+im\,\mathrm{Im}(\mathbf{u}_{Ah})]\cdot[\mathrm{Re}(\mathbf{u}_{Aj})+in\,\mathrm{Im}(\mathbf{u}_{Aj})])\\&\times([\mathrm{Re}(\mathbf{u}_{Ak})-im\,\mathrm{Im}(u_{Ak})]\cdot[\mathrm{Re}(\mathbf{u}_{Al})-in\,\mathrm{Im}(\mathbf{u}_{Al})]).\end{aligned} \tag{49}$$

The expression for the Alfvén pump wave energy density is

$$\varepsilon_A=\frac{\rho_0}{4H}\sum_{h=1}^{H}\sum_{j=1}^{H}\sum_{m=\pm1}\sum_{n=\pm1}\delta_{mk_h,nk_j}\delta_{m\omega_h,n\omega_j}\exp(i(m\phi_h-n\phi_j))\times[\mathrm{Re}(\mathbf{u}_{Ah})+im\,\mathrm{Im}(\mathbf{u}_{Ah})]\cdot[\mathrm{Re}(\mathbf{u}_{Aj})-in\,\mathrm{Im}(\mathbf{u}_{Aj})]. \tag{50}$$

In Eqs. (50) and (51), the well-known relation between the Dirac and Kronecker delta functions is used. Dividing Eq. (49) by Eq. (50) yields the desired rate of energy dissipation, ν. Upon taking ensemble averages over the random phases, ϕ_h, in each term in the sums in the preceding equations, all cross terms vanish. Upon defining new quantities in terms of the driven modes, $\mathbf{k}_{hjmn}=m\mathbf{k}_h+n\mathbf{k}_j$, and the angles, θ_{hjmn}, between these vectors and $\mathbf{B}_0$, we obtain Eq. (51). A similar expression, Eq. (52), is obtained for the coupling efficiency, ι, defined below, which depends only upon the ratio of the fluctuating amplitude, $|\mathbf{u}_A|$, to the background Alfvén speed, v_A, the plasma beta, β, and the angle of propagation of the driven wave, θ_{hjmn}:

$$\nu=\frac{\xi_M}{\varepsilon_A}=\frac{1}{16H\Sigma_{h=1}^{H}\Sigma_{m=\pm1}|\mathrm{Re}(\mathbf{u}_{Ah})+m\,\mathrm{Im}(\mathbf{u}_{Ah})|^2}\sum_{h=1}^{H}\sum_{j=1}^{H}\sum_{m=\pm1}\sum_{n=\pm1}\sum_{N=1}^{2}C_{MN}(\theta_{hjmn})$$
$$\times\frac{d_{2N}(\eta[\theta_{hjmn}])k_{hjmn}v_A^3|\hat{\mathbf{u}}_N\cdot\hat{\mathbf{k}}_{hjmn}|^2}{\Pi_{Z=1}^{2}|v_A\cos\theta_{hjmn}+[1+id_{ZN}(\eta[\theta_{hjmn}])]p(Z,N,\theta_{hjmn})|^2}\times|[\mathrm{Re}(\mathbf{u}_{Ah})+im\,\mathrm{Im}(\mathbf{u}_{Ah})]\cdot[\mathrm{Re}(\mathbf{u}_{Aj})$$
$$+in\,\mathrm{Im}(\mathbf{u}_{Aj})]|^2 \tag{51}$$

and

$$\iota=\frac{\varepsilon_M}{\varepsilon_A}=\frac{1}{32H\Sigma_{h=1}^{H}\Sigma_{m=\pm1}|\mathrm{Re}(\mathbf{u}_{Ah})+m\,\mathrm{Im}(\mathbf{u}_{Ah})|^2}\sum_{h=1}^{H}\sum_{j=1}^{H}\sum_{m=\pm1}\sum_{n=\pm1}\sum_{N=1}^{2}C_{MN}(\theta_{hjmn})$$
$$\times\frac{v_A^2|\hat{\mathbf{u}}_N\cdot\hat{\mathbf{k}}_{hjmn}|^2}{\Pi_{Z=1}^{2}|v_A\cos\theta_{hjmn}+[1+id_{ZN}(\eta[\theta_{hjmn}])]p(Z,N,\theta_{hjmn})|^2}\times|[\mathrm{Re}(\mathbf{u}_{Ah})+im\,\mathrm{Im}(\mathbf{u}_{Ah})]\cdot[\mathrm{Re}(\mathbf{u}_{Aj})$$
$$+in\,\mathrm{Im}(\mathbf{u}_{Aj})]|^2. \tag{52}$$

Expressions for the dot products of the unit eigenvectors with $\mathbf{k}$ follow from Eqs. (21) and (22):

$$\hat{\mathbf{u}}_1\cdot\hat{\mathbf{k}}=\frac{(p^2(2,1)-v_A^2)\cos\theta}{\sqrt{(p^2(2,1)-v_A^2-c_s^2\sin^2\theta)^2+c_s^4\sin^2\theta\cos^2\theta}} \tag{53}$$

and

$$\hat{\mathbf{u}}_2\cdot\hat{\mathbf{k}}=\frac{p^2(2,2)\sin\theta}{\sqrt{(p^2(2,2)-c_s^2\cos^2\theta)^2+c_s^4\sin^2\theta\cos^2\theta}}. \tag{54}$$

It is useful to observe how ι and ν in Eqs. (51) and (52) vary with β and θ_{hjmn}. For the sake of obtaining a simple graphical result to illustrate the physics, only the beating of a pair of waves is considered here, leaving more complicated cases for future investigation. We show in Figs. 2 and 3 how ι depends upon θ_{hjmn}, for several values of beta. Note that ι is independent of k_{hjmn}, and that it is normalized by the dimensionless total strength of the Alfvén waves, $|\mathbf{u}_A|^2/v_A^2$. The expressions, $C_M\sim 2,d$, and $p(Z,N)$ are defined in Eqs. (42), (37), and (33), respectively. It should be noted that the imaginary part of the phase velocity of damped waves is always negative, and that the plots in Figs. 2 and 3 are symmetric about $\pi/2$.

Figure 2 indicates that energy is most efficiently coupled into driven fast magnetosonic modes that propagate obliquely and nearly along $\mathbf{B}_0$. For any given Alfvén wave of fixed finite amplitude and direction, the matching conditions in Sec. II imply that nearly resonant magnetosonic waves will be produced by the interaction with a second wave whose wave vector lies along a specific trajectory in Euclidean space. Each of the four matching conditions, two of which are redundant, produces a trajectory in Euclidean space. Thus, a particular Alfvén wave can be damped due to an interaction with many different Alfvén waves, but only with those Alfvén waves that lie within a specific region in phase space. An interesting question for future work is how this will affect the evolution of some initial Alfvén wave spectrum over time.

Furthermore, the energy dissipation rate can be inferred by comparing Eqs. (51) and (52). Hence, $\nu\sim 2\iota d_{2N}k_{hjmn}\,v_A\cos\theta_{hjmn}\sim 2\iota d_{2N}\omega_{hjmn}$. Note that ω_{hjmn} is the frequency of the resonantly driven wave. It is also a good

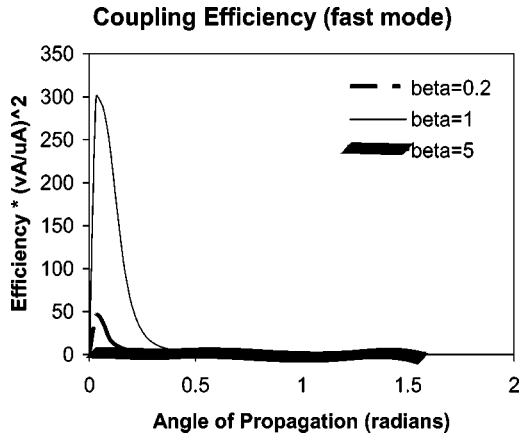

FIG. 2. Fast mode coupling efficiency as a function of the direction of driven waves.

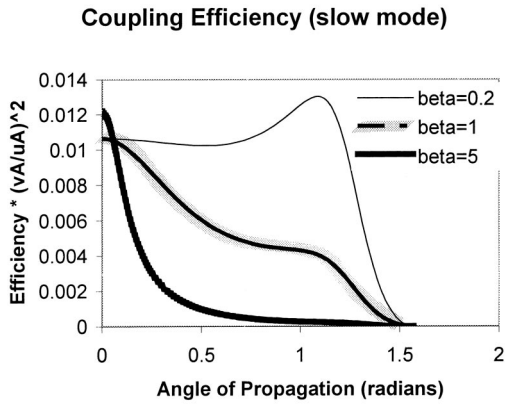

FIG. 3. Slow mode coupling efficiency as a function of the direction of driven waves.

approximation to the frequency of nearly resonant driven waves. As the wave number and, thus, the frequency increase, damping occurs more rapidly in absolute terms. In addition, the damping rate is proportional to the square of the Alfvén wave amplitude, so that the damping slows down as the waves dissipate.

We now consider some specific examples. In the solar wind, the largest wave number in the energy-containing part of the spectrum, the region where the observed wave amplitude is fairly constant, decreases substantially as the distance from the sun increases. For heliocentric distances less than 1 a.u., it is typically[28] on the order of 10^{-9} m^{-1}. At 5 a.u., this critical wave number is already smaller[29] than 10^{-10} m^{-1}. The typical ratio, $|\mathbf{u}_A|/v_A \sim |\delta\mathbf{B}|/\mathbf{B}_0$, is 0.55. Using these parameters and Figs. 2 and 3, ν can be evaluated for some value of β.

It is not uncommon to find $\beta \sim 1$ in the solar wind. This is known to occur in the sunspot region in the photosphere and lower chromosphere, in the plage region in the lower and middle corona (1.2 solar radii) and in significant portions of the upper corona and solar wind.[30] When $\beta \sim 1$, the resonant value of d_{22}, corresponding to the fast magnetosonic mode, is no greater than 10^{-2}. As mentioned before, the resonance seen in Fig. 2 occurs for driven waves that propagate nearly along $\mathbf{B}_0$. For these numbers, $\nu/\omega_{hjmn} \sim 1$, which corresponds to a damping time of a few hours for waves with $k \sim 10^{-9}$ m, where $v_A \sim 50$ km/s (as is is typical for the corona and the solar wind within 1 a.u.). As the distance from the Sun increases, this damping time will tend to increase as v_A decreases and as the maximum k in the energy-containing part of the Alfvén-wave spectrum decreases, but it will tend to decrease if $|\delta\mathbf{B}|/\mathbf{B}_0$ increases as $\mathbf{B}_0$ decreases. Even so, wherever $\beta \sim 1$ one would expect the spectrum of Alfvénic turbulence will evolve quite rapidly, with corresponding plasma heating. The existence of very strong Alfvén-wave damping for $\beta \sim 1$ could also be very important in other astrophysical contexts.

However, β does not have to drop much below 1 before the damping by the mechanism described here becomes much smaller and probably unimportant. In particular, it is also not uncommon to encounter $\beta \sim 0.2$ in the solar wind, particularly at heliocentric distances of 5–20 solar radii. For this case, the resonant value of d_{22} is 10^{-4}. In this case $\nu/\omega \approx 3 \times 10^{-3}$, which corresponds to a damping time on the order of a year for waves with $k \sim 10^{-9}$ m, where $v_A \sim 50$ km/s. Thus, for such "low-β" regions of the solar wind, this process would be expected to contribute only marginally to the evolution of turbulence. It could limit the increase of $|\delta\mathbf{B}|/B_0$ at a few a.u., where timescales are days and where $\mathbf{B}_0$ may be decreasing more rapidly than $|\delta\mathbf{B}|/B_0$. Nonetheless, it might contribute to ion heating in the outer regions of the heliosphere.

The damping decreases strongly again when the plasma beta exceeds unity, although it is not clear that this has direct relevance to the solar wind. For example, when $\beta = 5$, the partially resonant slow mode dominates the interaction, d_{21}, which is approximately 0.5, can be used in the place of d_{22}. In this case $\nu/\omega \approx 3 \times 10^{-3}$. This suggests a potential feedback mechanism in $\beta \sim 1$ plasmas that contain significant Alfvénic turbulence. The damping will heat the plasma just enough to keep β above 1 and drive down the damping rate. This feedback process could control the temperature of plasmas that are attempting to cool by expansion or radiation. It could also mean that plasmas that begin as high-β systems and then expand or radiate actively will effectively burn up their Alfvénic turbulence in the process.

VI. CONCLUSION

In this paper, the Alfvén wave population has been suggested as a possible source of energy for solar wind heating and acceleration. In particular, as plasma expands radially outward, the beating of the Alfvén waves transfers energy through magnetosonic waves to the particles, potentially affecting the bulk flow velocity, the particle distributions, and the Alfvén wave spectrum. As energy is transferred away from the fluctuations, their overall amplitude decays. Alfvénic turbulence is always present in the solar wind as a consequence of nearly incompressible MHD and, indeed, the total energy carried by Alfvén waves is observed to decrease as heliospheric distance increases.

As is discussed in the preceding sections, the nonlinear coupling of Alfvén pump waves with the slow magnetosonic mode results in a rather weak response with characteristic times on the order of a year for all driven-wave propagation angles. On the other hand, interaction with the fast mode results in very rapid dissipation on the order of hours for very particular angles of propagation, when optimal pairs of Alfvén waves having typical wave vector magnitudes beat to produce the driven wave and when the plasma β is near unity. This occurs when the driven wave approaches a resonance in the fast magnetosonic dispersion relation. The strength of the response drops off very rapidly away from this resonance. All Alfvén waves can beat with some other Alfvén waves to produce driven waves near the resonant angle, but the net damping is reduced in proportion to the magnitude of the driven wave vector and the Alfvén wave amplitudes. The work presented in this document can form the basis for calculations of the evolution of realistic Alfvén wave distributions and the heating that will result. A natural extension of the present work would be to use kinetic theory to replace the approximate damping rates used here with more realistic damping rates for the driven modes. The important conclusion of this work is that the impact of magnetosonic waves on the evolution and damping of the Alfvén waves cannot be ignored if the plasma β is near unity. This potentially could have broad applications in the heliosphere and elsewhere in astrophysics.

This Alfvén-wave-beating mechanism might explain certain local effects in particular spectra such as the preacceleration of superthermal particle populations, which are present in the fast stream of the solar wind. Upon being heated, these energetic tails can lead to the stochastic acceleration of the fast solar wind in regions where shocks form. This latter mechanism has a broad range of applicability in fast and slow streams. In order for a mechanism to create these high-energy tails, the characteristic time for dissipation must be on the order of 10^5 s[5]. The dissipation rates de-

scribed in this paper suggest that the Alfvén-wave-beating mechanism may be a candidate for explaining the preacceleration.

ACKNOWLEDGMENTS

The authors acknowledge extensive and useful discussions with Professor Ziyaeddin A. Ackasu of the University of Michigan and with Dr. Nathan Schwadron of Southwest Research Institute. In addition, Dr. Schwadron contributed to the analysis of the magnetosonic eigenmodes.

[1]C.-Y. Tu and E. Marsch, *MHD Structures, Waves and Turbulence in the Solar Wind* (Kluwer Academic, Dordrecht, The Netherlands, 1995).
[2]W. H. Matthaeus, G. P. Zank, C. W. Smith, and S. Oughton, Phys. Rev. Lett. **82**, 3444 (1999).
[3]S. R. Spangler, Astrophys. J. **522**, 879 (1999).
[4]S. H. Bekhor, Ph.D. thesis, University of Michigan, 2002.
[5]E. N. Parker, Astrophys. J. **128**, 664 (1958).
[6]T. E. Holzer, in *Solar System Plasma Physics*, edited by C. F. Kennel, L. J. Lanzerotti, and E. N. Parker (North-Holland, New York, 1979), p. 101.
[7]A. O. Benz, *Plasma Astrophysics: Kinetic Processes in Solar and Stellar Coronae* (Kluwer Academic, Dordrecht, The Netherlands, 1993), p. 12.
[8]I. K. Khabibrakhmanov and D. J. Mullan, Astrophys. J. **430**, 814 (1994).
[9]I. Cuseri, D. J. Mullan, G. Noci, and G. Poletto, Astrophys. J. **514**, 989 (1999).
[10]L. A. Fisk, G. Gloeckler, T. H. Zurbuchen, and N. A. Schwadron, in *ACE 2000 Symposium*, edited by R. A. Mewaldt, J. R. Jokipii, M. A. Lee, E. Mobius, and T. A. Zurbuchen (American Institute of Physics, Melville, NY, 2000), p. 229.
[11]M. V. Medvedev and P. H. Diamond, Phys. Plasmas **3**, 863 (1996).
[12]M. V. Medvedev, P. H. Diamond, V. I. Shevchenko, and V. L. Galinsky, Phys. Rev. Lett. **78**, 4934 (1997).
[13]M. V. Medvedev and P. H. Diamond, Phys. Rev. E **56**, 2371 (1997).
[14]R. H. Kraichnan, Phys. Fluids **8**, 1385 (1965).
[15]J. Fleischer and P. H. Diamond, Phys. Rev. E **58**, 2709 (1998).
[16]P. Goldreich and S. Sridhar, Astrophys. J. **438**, 763 (1995).
[17]J. Y. Cho and A. Lazarian, Phys. Rev. Lett. **88**, 245001 (2002).
[18]G. M. Webb, A. R. Zakharian, M. Brio, and G. P. Zank, J. Plasma Phys. **66**, 167 (2001).
[19]P. K. Kaw, W. L. Kruer, C. S. Liu, and K. Nishikawa, *Advances in Plasma Physics* (Wiley, New York, 1976).
[20]A. Barnes, Phys. Fluids **9**, 1483 (1966).
[21]M. L. Goldstein, Astrophys. J. **219**, 700 (1978).
[22]A. F. Viñas and M. L. Goldstein, J. Plasma Phys. **46**, 107 (1991).
[23]A. F. Viñas and M. L. Goldstein, J. Plasma Phys. **46**, 129 (1991).
[24]D. R. Nicholson, *Introduction to Plasma Theory* (Kreiger, Malabar, FL, 1992).
[25]M. L. Goldstein, C. W. Smith, and W. H. Matthaeus, J. Geophys. Res., [Space Phys.] **88**, 9989 (1983).
[26]G. P. Zank and W. H. Matthaeus, Phys. Fluids A **5**, 257 (1993).
[27]C. Y. Tu and E. Marsch, J. Geophys. Res., [Space Phys.] **99**, 21481 (1994).
[28]M. L. Goldstein, D. A. Roberts, and W. H. Matthaeus, Annu. Rev. Astron. Astrophys. **33**, 283 (1995).
[29]W. H. Matthaeus and M. L. Goldstein, J. Geophys. Res., [Space Phys.] **87**, 6011 (1982).
[30]G. A. Gary, Sol. Phys. **203**, 71 (2001).